

Q U I N T E S S E N T I A L K I N A T I O N A N D C O L D D A R K M A T T E R A B U N D A N C E

C . P A L L I S

Physics Division, School of Technology,
Aristotle University of Thessaloniki,
541 24 Thessaloniki, GREECE
e-mail address: kpallis@auth.gr

A B S T R A C T

The generation of a kination-dominated phase by a quintessential exponential model is investigated and the parameters of the model are restricted so that all the observational constraints (originating from nucleosynthesis, the present acceleration of the universe and the dark energy density parameter) are satisfied. The decoupling of a thermal cold dark matter particle during the period of kination or before its commencement is analyzed, the relic density is calculated both numerically and semi-analytically and the results are compared with each other. The enhancement, with respect to the standard paradigm, of the cold dark matter abundance is demonstrated in both regimes of decoupling and its variation with the quintessential parameters is examined. Fixing them to representative values, acceptable results for the cold dark matter abundance are obtained by constraining the mass and the thermal-averaged cross section times the velocity of the cold relic. Alternatively, in the case of the decoupling during the period of kination, the quintessential density parameter at the onset of nucleosynthesis can be further restricted model-independently by the data on the cold dark matter abundance.

Keyw ords: Cosm ology, D ark Energy, D ark M atter

P A C S C odes: 98.80.Cq, 98.80.-k, 95.35.+d

CONTENTS

1	INTRODUCTION	1
2	QUINTESENTIAL COSMOLOGY	3
2.1	RELEVANT EQUATIONS	3
2.2	QUINTESENTIAL DYNAMICS	5
2.3	QUINTESENTIAL REQUIREMENTS	6
3	CDM ABUNDANCE IN THE PRESENCE OF THE KD PHASE	7
3.1	THE BOLTZMANN EQUATION	7
3.2	NUMERICAL CALCULATION	8
3.3	SEMI-ANALYTICAL CALCULATION	8
4	APPLICATIONS	10
4.1	EVOLUTION OF THE QUINTESENTIAL QUANTITIES	10
4.2	IMPOSING THE QUINTESENTIAL REQUIREMENTS	13
4.3	PRE-VERSUS POST-FREEZE-OUT h_0^2 ENHANCEMENT	14
4.4	NUMERICAL VERSUS SEMI-ANALYTICAL RESULTS	14
4.5	IMPOSING THE CDM REQUIREMENT	17
5	CONCLUSIONS-OPEN ISSUES	20

1. INTRODUCTION

A plethora of recent data [1, 2] has indicated that the two major components of the present universe are the Cold (mainly [3]) Dark Matter (CDM) and the Dark Energy (DE) with density parameters [1], respectively:

$$(a) \quad \Omega_{\text{CDM}} = 0.24 \pm 0.01 \quad \text{and} \quad (b) \quad \Omega_{\text{DE}} = 0.73 \pm 0.02; \quad (1.1)$$

at 95% confidence level (c.l.). The identification of these two unknown substances consists one of the most tantalizing enigmas of the modern cosmology-particle theories.

As regards CDM, the most natural candidates [4], are the weakly interacting massive particles, The most popular of these, is the lightest supersymmetric (SUSY) particle (LSP) [5]. However, the extra dimensional (ED) theories give rise to new CDM candidates [6, 7, 8]. According to the standard cosmological scenario (SC) [9], $\tilde{\nu}_\tau$ decouples being non-relativistic from the cosmic fluid (i) during the radiation-dominated (RD) era, (ii) being in chemical equilibrium with plasma and (iii) produced through thermal scatterings in the plasma (note that these assumptions are, also, naturally valid in the case of the so-called second Randall-Sundrum [10] model, provided that the brane-tension is constrained to rather high values [11]). The viability of other CDM candidates (like axions [12], axino [14], gravitino [13], quintessino [15]) requires a somehow different cosmological set-up, which we do not consider in our analysis. In light of eq. (1.1), the relic density, $\Omega_{\tilde{\nu}_\tau} h_0^2$, is to satisfy the following range of values:

$$(a) \quad 0.09 \leq \Omega_{\tilde{\nu}_\tau} h_0^2 \leq 0.13 \quad \text{and} \quad (b) \quad \Omega_{\tilde{\nu}_\tau} h_0^2 \leq 0.13; \quad (1.2)$$

As regards DE, quintessence [16], the energy density of a slowly evolving scalar field, has recently attracted much attention (for reviews, see ref. [17]). The scalar field is supposed to roll down its potential undergoing three phases during its cosmological evolution: Initially its

kinetic energy, which decreases faster than the radiation, dominates and gives rise to a possible novel period in the universal history termed "kination" [18]. Then the scalar field freezes to a value close to M_P and by now its potential energy, adjusted so that eq. (1.1b) is met, becomes dominant. Such an adjustment, which certainly does not resolve satisfactorily the coincidence problem, is unavoidable in quintessential models (for related suggestions, see refs. [19, 20]). Other shortcomings such as the lightness of the scalar field [21] or the time variation of the gauge coupling constants [22] are currently under investigation.

Be that as it may, the viability of a quintessential scenario can be controlled by imposing some observational constraints [23], arising from nucleosynthesis, acceleration of the universe and the DE density parameter. Unfortunately no full-satisfactory potential exists, to date (for comparative explorations of various potentials, see refs. [24, 25]). E.g., the inverse power potential [26] although provides a tracker-type solution [27] does not fit well [28] the present-day value [1, 2] of the quintessence-equation-of-state parameter. Phenomenologically more robust [25] is the supergravity-inspired [28, 29] potential without, however, to allow a zero minimum of the potential [28, 3]. Also, in both cases, the generation in the early universe of a kination-dominated (KD) expansion consistent with the fulfillment of the requirements above is rather questionable [30, 31]. For these reasons, we decide to examine the simplest exponential potential [32, 29], which, although does not possess a tracker-type solution [27, 30], it can produce a viable present-day cosmology in conjunction with the domination of an early KD era, for a reasonable region of initial conditions [23, 25, 33].

The departure from the SC, caused by the implementation of a quintessential KD epoch can modify the h_0^2 calculation, which (as, already, emphasized [34, 35, 36]) crucially depends on the adopted assumptions. If the quintessential KD phase dominates over the radiation (a condition indispensable for the quintessential inflationary model building [37, 38, 39]), the assumption (i) of the SC is lifted (note that the assumptions (ii) and (iii) are maintained in our analysis). As a consequence, an increase to h_0^2 with respect to (w.r.t) its value in the SC is implied. This phenomenon was first pointed out in ref. [30] and was explored in ref. [40] for the parameters of the exponential potential, which support a global attractor [41]. There [40], h_0^2 was calculated numerically for a couple of SUSY models which resurrect higgsino [42] or wino [43] LSP and can yield acceptable h_0^2 .

Contrary to ref. [40], we focus on the range of the exponential-potential parameters, which ensures a late-time attractor together with an early KD regime (see sec. 2.2) and can lead to a simultaneous satisfaction of all the observational data (see secs. 2.3 and 4.2). We then, present a "unified" (using the same independent variable) description of both phenomena (the cosmological evolution of the quintessence field and the decoupling) (see, secs. 2.2 and 3.3). The relevant equations are solved both numerically (see secs. 2.1 and 3.2) and semi-analytically (see secs. 2.2 and 3.3) and the results are compared with each other (see secs. 4.1 and 4.4). We distinguish two specific mechanisms, which differently increase h_0^2 w.r.t the one in the SC (see sec. 4.3). Finally, we restrict the parameters in posing all the DE and CDM constraints, without, however, to adopt a specific particle model (see sec. 4.5).

The framework of the quintessential cosmology is described in detail in sec. 2, while our numerical and semi-analytical h_0^2 calculations are displayed in sec. 3. Some model-independent applications of our findings are realized in sec. 4. Finally, sec. 5 summarizes our results and discusses some open questions.

Throughout the text and the formulas, brackets are used by applying disjunctive correspondence, natural units ($\sim = c = k_B = 1$) are assumed, the subscript or superscript 0 is referred to present-day values and \ln [\log] stands for logarithm with basis e [10].

2. QUINTESSENTIAL COSMOLOGY

We briefly describe the equations which govern the evolution of the universe in the presence of quintessence (sec. 2.1), the phases which the quintessence field undergoes during its history (sec. 2.2) and the requirements which a successful quintessential scenario is to satisfy (sec. 2.3).

2.1. RELEVANT EQUATIONS

According to the quintessential scenario, we assume the existence of a spatially homogeneous, scalar field q (not to be confused with the deceleration parameter [3]) which obeys the Klein-Gordon equation. We below present its archetypal form and then we derive simplified forms which facilitate its numerical integration [23, 25]. Finally, we specify the used initial conditions and we define the useful extracted quantities.

2.1.1. Initial form. The homogeneous Klein-Gordon equation in a cosmological set-up is

$$(a) \quad \ddot{q} + 3H\dot{q} + V_{,q} = 0; \quad \text{where} \quad (b) \quad V = V_0 e^{-q/m_p} \quad (2.1)$$

is the adopted potential for the field q , dot [$\dot{}$] stands for derivative w.r.t the cosmic time $[q]$ and H is the Hubble expansion parameter,

$$(a) \quad H^2 = \frac{\rho_q + \rho_r + \rho_m}{3m_p^2} \quad \text{with} \quad (b) \quad \rho_q = \frac{1}{2}\dot{q}^2 + V; \quad (2.2)$$

the energy density of q and $m_p = M_p/8$, where $M_p = 1.22 \cdot 10^{19}$ GeV is the Planck scale. The energy density of radiation, ρ_r , can be evaluated as a function of temperature, T , whilst this of matter, ρ_m , with reference to its present-day value:

$$(a) \quad \rho_r = \frac{2}{30}g T^4 \quad \text{and} \quad (b) \quad \rho_m R^3 = \rho_m^0 R_0^3 \quad (2.3)$$

with R , the scale factor of the universe. Assuming no entropy production during the evolution of q , the following two equations are valid for the entropy density, s :

$$(a) \quad sR^3 = s_p R_p^3 \quad \text{where} \quad (b) \quad s = \frac{2}{45}g_s T^3; \quad (2.4)$$

where p represents a specific reference point at which the constant quantity sR^3 is evaluated and $g(T)$ [$g_s(T)$] is the energy [entropy] effective number of degrees of freedom at temperature T . Their numerical values are evaluated by using the tables included in micrOMEGAS [44], originated from the DarkSUSY package [45] (recent improvements [46] do not affect essentially the results). Useful numerical values for the present-day quantities are given in the next subsection.

2.1.2. Reformulation. The numerical integration of eq. (2.1) is facilitated by converting the time derivatives to derivatives w.r.t the logarithmic time [23, 25]:

$$\dot{q} = \ln(R/R_0) = \ln(1+z) \quad (\dot{\quad} = H): \quad (2.5)$$

with z , the redshift. Changing the differentiation, eq. (2.1) turns out to be equivalent to the system of two first-order equations:

$$(a) \quad Q = H\dot{q} \quad \text{and} \quad (b) \quad H\dot{Q} + 3HQ + V_{,q} = 0 \quad \text{with} \quad (c) \quad \rho_q = \frac{1}{2}Q^2 + V; \quad (2.6)$$

In terms of Q in eq. (2.6), s and T can be expressed through the relations:

$$(a) \quad s = s_0 e^{3Q} \quad \text{and} \quad (b) \quad T = T_0 \left(\frac{g_s^0}{g_s}\right)^{1/3} e^{-Q}; \quad (2.7)$$

where eqs. (2.4a) and (2.4b) have been used. Similarly, ρ_R and ρ_M are elegantly cast in the form :

$$(a) \quad \rho_R = \frac{\rho_R^0 g}{g^0} \left(\frac{g_s^0}{g_s} \right)^{4=3} e^4 \quad \text{and} \quad (b) \quad \rho_M = \frac{\rho_M^0}{M} e^3 ; \quad (2.8)$$

where eq. (2.7b) has been inserted in eq. (2.3a) and eq. (2.5) has been combined with eq. (2.3b).

2.1.3. Normalized form . An even more "robust" [25] form of eq. (2.6) can be achieved, if we introduce the following dimensionless quantities:

$$(a) \quad \rho_{R[M]} = \frac{\rho_{R[M]}^0}{\rho_c^0}; \quad (b) \quad V_o = V_o = \frac{V_o^0}{c} \quad \text{and} \quad (c) \quad q = \frac{q^0}{3m_p} \quad (2.9)$$

Substituting these quantities in eq. (2.6), this can be re-written:

$$(a) \quad Q = H q^0 \quad \text{and} \quad (b) \quad H Q^0 + 3H Q + V_{q1} = 0 \quad \text{with} \quad (c) \quad H^2 = \frac{H^2}{q + \rho_R + \rho_M}; \quad (2.10)$$

where the following quantities have been defined:

$$(a) \quad V = V_o e^{\frac{p}{3} q}; \quad H = H = H_0; \quad Q = Q = \frac{Q^0}{c} \quad \text{and} \quad (b) \quad \frac{H^2}{q} = Q^2 = 2 + V; \quad (2.11)$$

In our numerical calculation, we use the following values:

$$\rho_c^0 = 8.099 \cdot 10^{47} h_0^2 \text{ GeV}^4 \quad \text{and} \quad H_0 = 2.13 \cdot 10^{42} h_0 \text{ GeV}; \quad (2.12)$$

with $h_0 = 0.72$. Also, $\rho_M^0 = 0.29$ and $T_0 = 2.35 \cdot 10^{13} \text{ GeV}$. Substituting the latter in eq. (2.3a), we obtain $\rho_R^0 = 8.04 \cdot 10^5$.

2.1.4. Extracted quantities. The measurable quantities which are used in order to restrict the parameters of the quintessential model (see sec. 2.3) are the density parameters of the q -eld, radiation and matter

$$\Omega_i = \Omega_i = (\rho_i / \rho_c) = \Omega_i = H^2; \quad \text{where} \quad i = q; R \quad \text{and} \quad M; \quad (2.13)$$

respectively and the barotropic index (or the equation-of-state parameter) of q -eld, w_q ,

$$w_q = (q^2 - 2 - V) / (q^2 - 2 + V) = 1 - \frac{2V}{q^2 - 2 + V}; \quad (2.14)$$

2.1.5. Initial Conditions. In order to solve eq. (2.10) two initial conditions are needed to be specified: These could be the values of q and q^0 at an initial t_i [23]. However, the result $q(t_i) = q_i \neq 0$ is equivalent as if we had $q(t_i) = 0$ and rescaled V_o to $V_o \exp(\frac{p}{3} q_i)$ [23]. So, without any loss of generality we take $q(t_i) = 0$ throughout our investigation. On the other hand, the value of $q^0(t_i)$ is not a suitable initial condition for our purposes. This is, because we wish to focus on the regime (see eqs. (2.13), (2.11b) and (2.10a)):

$$q(t_i) \ll \frac{H_I^2 q^0(t_i) = 2}{H_I^2}, \quad 1 \gg q^0(t_i) \ll \frac{p}{2}; \quad (2.15)$$

where we take $\Omega_{qI} = \Omega_{qI} = \frac{H_I^2 q^0(t_i) = 2}{H_I^2}$ and $H_I = H(t_i)$. This means that $Q_I = Q(t_i)$ tends to infinity, since from eqs. (2.10c) we obtain:

$$Q = \frac{H_I^2}{3} \frac{V + \rho_R + \rho_M}{1 - Q^2 = 2} \quad (2.16)$$

In order to handle properly this subtlety, we find it convenient to define as initial condition, the square root of the kinetic-energy density of q at t_i ,

$$p \frac{H_I^2}{2} = Q(t_i) = \frac{p}{2} \frac{H_I^2}{q_i}; \quad (2.17)$$

2.2. QUINTESENTIAL DYNAMICS

We can obtain a comprehensive and rather accurate approach of the q dynamics, following the arguments of ref. [39]. Namely, q undergoes the following three phases:

2.2.1. Kinetic-Energy Dominated Phase. During this phase, the evolution of both the universe and q is dominated by the kinetic energy density of q . Consequently, eq. (2.10a) reads:

$$(a) \ H \dot{Q} + 3H Q = 0 \quad \text{with} \quad (b) \ H^2 = \frac{1}{2} \dot{q}^2 \quad (2.18)$$

The former equation can be integrated trivially, with result:

$$Q = Q_I e^{3(\tau - \tau_I)} \quad \dot{q} = \dot{q}_I e^{6(\tau - \tau_I)} \quad (2.19)$$

Combining eq. (2.18b) with (2.10), we obtain:

$$\frac{1}{2} \dot{q}^2 - \frac{1}{2} \dot{q}_I^2 = \frac{1}{2} \dot{q}_I^2 \left(e^{6(\tau - \tau_I)} - 1 \right) \quad \text{for} \quad \tau < \tau_{KR} \quad (2.20)$$

with τ_{KR} , the point where the totally KD phase is terminated. This occurs, when:

$$\tau_{KR} = \tau_I + \ln \frac{g_{RI}}{g_{KR}} \quad (2.21)$$

where g_{RI} in eq. (2.19) has been equated at τ_{KR} with the following expression for g_{RI} ,

$$g_{RI} = \frac{g_{KR}}{g_{KR}^I} e^{4(\tau_{KR} - \tau_I)} \quad (2.22)$$

Eq. (2.4a) with reference point τ_I and eq. (2.3a) are employed in order to extract eq. (2.22), supposing that g_{KR} are not vary from their values at τ_I , $g_{KR}^I = g_{KR}(\tau_I)$.

2.2.2. Frozen-Field Dominated (FD) Phase. For $\tau > \tau_{KR}$, the universe becomes RD but the evolution of q continues to be dominated by its kinetic energy density. Therefore,

$$(a) \ H \dot{Q} + 3H Q = 0 \quad \text{with} \quad (b) \ H^2 = \frac{1}{2} \dot{q}^2 \quad (2.23)$$

Inserting eq. (2.23b) into eq. (2.10a) and integrating the resulting, we obtain:

$$\dot{q} = \dot{q}_{KR} + \frac{1}{2} \dot{q}_{KR}^2 \frac{1}{\dot{q}_{KR}} \left(e^{6(\tau - \tau_{KR})} - 1 \right) \quad \text{for} \quad \tau < \tau_{FA} \quad (2.24)$$

where $\dot{q}_{KR} = \dot{q}(\tau_{KR}) = \ln \left(\frac{g_{KR}}{g_{KR}^I} \right) = \frac{1}{2} \dot{q}_{KR}^2$ from eqs. (2.20) and (2.21) and τ_{FA} is specified in eq. (2.29). It is obvious from eq. (2.24) that q freezes at about $\tau_{KF} = \tau_{KR} + 6$ to the value:

$$\dot{q}_{KF} = \dot{q}_{KR} + \frac{1}{2} \dot{q}_{KR}^2 \left(e^{6(\tau_{KF} - \tau_{KR})} - 1 \right) \quad \text{for} \quad \tau_{KF} < \tau_{FA} \quad (2.25)$$

Note that \dot{q} reaches its constant value, $\dot{q}_{FA} = V(\dot{q}_{FA})$, at $\tau_{PL} = \tau_{KF}$ such, that:

$$V(\dot{q}_{PL}) = V(\dot{q}_{FA}) = \frac{1}{2} \dot{q}_{FA}^2 \quad \tau_{PL} = \tau_I + \frac{1}{2} \ln \left(\frac{g_{KR}}{g_{KR}^I} \right) = 6 \quad (2.26)$$

2.2.3. Attractor Dominated (AD) Phase. For $\tau > \tau_{PL}$, q becomes V dominated as in the case of inflation. Consequently, the evolution of q is described by the following:

$$(a) \ 3H \dot{Q} + V_{,q} = 0 \quad \text{with} \quad (b) \ H^2 = \frac{1}{3} \dot{q}^2 e^{3(1+w_B)\tau} \quad (2.27)$$

where τ_B is the dominant background-energy density of the universe with barotropic index $w_B = 1/3$ [0] for the RD [matter-dominated (MD)] era. As can be shown [32], and has been extensively discussed [23, 25, 33, 39], the system in eq. (2.1) admits:

- (i) A global attractor for $\omega > \frac{p}{3(1+w_B)}$ with a fixed-point barotropic index $w_q^{\text{fp}} = w_B$ and density parameter $\Omega_q^{\text{fp}} = 3(1+w_B)^{-2}$. This is the so-called self-tuning [27, 29, 41] case where the q evolution is insensitive to the choice of V_0 . However, this case can be discarded [23, 25] since, it fails to meet the observational data (see sec. 2.3).
- (ii) A late-time attractor for $\omega < \frac{p}{3(1+w_B)}$ with $w_q^{\text{fp}} = \frac{2}{3} - 1$ and $\Omega_q^{\text{fp}} = 1$. As is pointed out [23, 25] and we verify in sec. 4.2, the model can satisfy all the observational constraints, for a reasonable set of initial conditions.

Inserting eq. (2.10a) into eq. (2.27a) and integrating the resulting, we obtain for the later case:

$$\ln q = \frac{p}{3} \bar{\omega} + \ln(V_0 = \Omega_q^0) = \frac{p}{3} \bar{\omega} \quad () \quad q^0 = \frac{p}{3} \bar{\omega} \quad \text{for } \omega > \omega_{\text{FA}} \quad (2.28)$$

where the transition from the FD to the AD phase occurs at the point ω_{FA} , which can be estimated by:

$$\omega_{\text{FA}} = \frac{p}{6} + \frac{p}{3} \bar{\omega}_{\text{KR}} = \ln(V_0 = \Omega_q^0) = \frac{2}{3} \quad (2.29)$$

The latter can be easily extracted by equating the values of the expressions in eqs. (2.24) and (2.28) for $\omega = \omega_{\text{FA}}$. Employing eq. (2.28), we can derive Q via eq. (2.10a). Inserting it in the relation $\Omega_q = Q^2 = (1+w_q)$, which can be derived from eq. (2.14), we arrive at the energy density of the late-time attractor:

$$\Omega_A^0, \quad \Omega_q^0 e^{3(1+w_q^{\text{fp}})} \quad \text{with } w_q^{\text{fp}} = \frac{2}{3} - 1 \quad (2.30)$$

2.3. QUINTESSENTIAL REQUIREMENTS

We briefly describe the various criteria that we impose on our quintessential model.

2.3.1. **KD \Constraint".** For the aims of the present paper, we desire to focus our attention on the range of parameters which ensure a domination of the q -kinetic energy at t_I . This can be achieved, relatively [absolutely], when:

$$(a) \quad \Omega_q(t_I) \leq 0.5 \quad [(b) \quad \Omega_q(t_I) = 1] \quad (2.31)$$

Ranges of parameters not restricted by eq. (2.31), which meet all the residual constraints of this section, are exploited in ref. [23].

2.3.2. **Nucleosynthesis (NS) Constraint.** The presence of q has not to spoil the successful predictions of Big Bang NS which commences at about $t_{\text{NS}} = 22.5$ corresponding (see eq. (2.7b)) to $T_{\text{NS}} = 1 \text{ MeV}$ [47]. Taking into account the most up-to-date analysis of ref. [47], we adopt a rather conservative upper bound on $\Omega_q(t_{\text{NS}})$, less restrictive than that of ref. [48]. Namely, we require:

$$\Omega_q^{\text{NS}} = \Omega_q(t_{\text{NS}}) \leq 0.21 \quad (95\% \text{ c.l.}) \quad (2.32)$$

which corresponds to additional effective neutrinos species $N_{\text{eff}} < 1.6$ [47]. Let us note that extra contributions in the left hand side of eq. (2.32) due to energy density of gravitational waves (GWs) created during the transition from the KD to RD era is negligible as we infer by explicitly applying the formulae of ref. [50]. On the other hand, we do not consider contributions (potentially large [49]) due to GWs generated during a possible former transition from inflation to KD epoch. The reason is that inflation could be driven by another field different to q and so, any additional constraint arisen from this period would be highly model dependent.

2.3.3. Coincidence Constraint. The present value of q_0 , \dot{q}_0 , must be compatible with the preferred range of eq. (1.1a). This can be achieved by adjusting the value of V_0 . Since, this value does not affect crucially our results (especially on the CDM abundance), we decide to fix \dot{q}_0 to its central experimental value, demanding:

$$\dot{q}_0 = \ddot{q}_0 = 0.73: \quad (2.33)$$

2.3.4. Acceleration Constraint. A successful quintessence scenario has to account for the present-day acceleration of the universe, i.e. [1],

$$1 - w_q(0) = 0.78 \quad (95\% \text{ c.l.}): \quad (2.34)$$

In addition, since the string theory disfavors the eternal acceleration, it would be desirable to demand $w_q^{\text{fp}} > -1$ [39]. However, in the case of the used potential, we did not succeed to achieve compatibility of the later optional restriction with eq. (2.34), in accordance with the findings of ref. [25].

In our scanning, finally, we take into account the following less restrictive but also non-rigorous bounds, which, however, do not affect crucially our results, since the used values in our calculation lie well far away from these:

$$(a) \quad 50 < \tau \quad \text{and} \quad (b) \quad H_{\text{I}} < 10^{56}: \quad (2.35)$$

Eq. (2.35a) comes from the gravitino constraint [51] which provides an upper bound on the reheat temperature, $T_{\text{RH}} < (10^9 - 10^{10}) \text{ GeV}$. This can be translated to a lower bound on τ , through eq. (2.7b). However, this bound may not be so reliable, since there is no thorough investigation of the gravitino constraint within the context of quintessence cosmology, to date. The bound of eq. (2.35b) comes from the COBE constraints [52] on the spectrum of GWs produced at the end of inflation [38].

3. CDM ABUNDANCE IN THE PRESENCE OF THE KD PHASE

We assume that the CDM candidate, χ , maintains kinetic and chemical equilibrium [34] with plasma, is produced through thermal scatterings and decouples during the KD epoch or before its commencement (obviously, if χ decouples after the termination of the KD era, the h_0^2 calculation reduces to the one used in the SC [9]). Our theoretical analysis is presented in sec. 3.1 and its numerical treatment in sec. 3.2. Useful approximated expressions are derived in sec. 3.3.

3.1. THE BOLTZMANN EQUATION

Since the χ particles are in kinetic equilibrium with the cosmic fluid, their number density, n , satisfies the following Boltzmann equation:

$$\dot{n} + 3Hn + \langle h \nu \rangle n^2 - n^{\text{eq}2} = 0; \quad (3.1)$$

where H is given by eq. (2.2a), $\langle h \nu \rangle$ is the thermal-averaged cross section of χ particles times the velocity and n^{eq} is the equilibrium number density of χ , which obeys the Maxwell-Boltzmann statistics:

$$n^{\text{eq}}(x) = \frac{g}{(2\pi)^{3/2}} m^{-3} x^{3/2} e^{-1/x} P_2(1/x); \quad \text{where } x = T/m \quad (3.2)$$

with m the mass of χ . We pose $g = 2$ for the number of degrees of freedom of χ and $P_n(z) = 1 + (4n^2 - 1)z$ is obtained by asymptotically expanding the modified Bessel function of the second kind of order n . Note that the production of χ 's, not being in chemical equilibrium with the cosmic fluid, requires $h \nu_i < 10^{20} \text{ GeV}^2$ [34]. Since such a value is well below the usually obtainable values [6, 7, 8, 34], we do not consider further this possibility, here.

3.2. NUMERICAL CALCULATION

Following the strategy of sec. 2.1.3, we introduce the dimensionless quantities:

$$Y^{\text{eq}} = \frac{n^{\text{eq}}}{g}; \text{ where } n^{\text{eq}} = m \frac{P_n}{h \nu_i}; \quad (3.3)$$

In terms of these, eq. (3.1) takes the following master, for numerical manipulations, form:

$$H^0 + 3H + \frac{d}{dx} \ln \nu_i^2 - Y^{\text{eq}2} = 0; \quad (3.4)$$

where H is given by eq. (2.10c) and the following quantities have been defined:

$$\frac{d}{dx} \ln \nu_i = \frac{P_n}{h \nu_i} \text{ and } m = m_{\text{eff}} = 3m_{\text{P}}; \quad (3.5)$$

Eq. (3.4) can be solved numerically with initial condition $Y(x_B) = Y^{\text{eq}}(x_B)$, where x_B corresponds (see eq. (2.7b)) to the beginning ($x = 1$) of the Boltzmann suppression of Y^{eq} . When $x_I < x_B$, the integration of eq. (3.4) is realized from x_B down to 0. When $x_B < x_I$, the integration is realized successively from x_B to x_I (posing $Y_q = 0$ into eq. (2.10c) for deriving H) and then from x_I down to 0. Finally, h_0^2 can be easily found, via the relation:

$$h_0^2 = (0)h_0^2; \quad (3.6)$$

3.3. SEMI-ANALYTICAL CALCULATION

The aim of this section is the calculation of h_0^2 based on the already obtained semi-analytical expressions of sec. 2.2. The procedure is described step-by-step below.

3.3.1. Reformulation of the Boltzmann Equation. Introducing the variables $Y^{\text{eq}} = n^{\text{eq}}/g$ [9, 54] (in order to absorb the dilution term) and converting the derivatives w.r.t t , to derivatives w.r.t x , eq. (3.1) can be rewritten as:

$$H Y^0 = \frac{d}{dx} \ln \nu_i Y^2 - Y^{\text{eq}2}; \quad (3.7)$$

where eq. (2.7a) has been also utilized. Substituting eqs. (2.22) and (2.19) in eq. (2.10c) and ignoring the negligible, during the decoupling, contribution of m , H can be expressed as:

$$(a) H^2 = \frac{g_{\text{R}}}{g_{\text{q}}} = 3m_{\text{P}}^2; \text{ where } (b) g_{\text{q}} = 1 + r_{\text{q}} \text{ with} \quad (3.8)$$

$$r_{\text{q}} = r_{\text{I}} \frac{g_{\text{I}}}{g} \frac{g_{\text{s}}^{4=3}}{g_{\text{I}}^{4=3}} e^{2(x_{\text{I}})} \text{ and } r_{\text{I}} = \frac{r_{\text{I}}}{g_{\text{I}}} \quad (3.9)$$

or, equivalently, taking as reference point x_{NS} instead x_{I} ,

$$r_{\text{q}} = r_{\text{NS}} \frac{g^{\text{NS}}}{g} \frac{g_{\text{s}}^{4=3}}{g_{\text{s}}^{\text{NS}}} e^{2(x_{\text{NS}})} \text{ with } r_{\text{NS}} = \frac{g_{\text{q}}^{\text{NS}}}{1 - g_{\text{q}}^{\text{NS}}} \quad (3.10)$$

and $g^{\text{NS}} = [g_{\text{s}}^{\text{NS}}]$, the values of $g = [g_{\text{s}}]$ at x_{NS} . Inserting eqs. (3.8), (2.8a) and (2.7a) into eq. (3.7), this can be cast in the following form:

$$Y^0 = \frac{Y h \nu_i}{g_{\text{q}}} Y^2 - Y^{\text{eq}2}; \text{ where} \quad (3.11)$$

$$Y(x) = \frac{s_0}{H_{\text{R}}^0} \frac{g^0}{g} \frac{g_{\text{s}}^{2=3}}{g_{\text{s}}^0} e^{x} \text{ with } H_{\text{R}}^0 = \frac{H_0}{H_{\text{R}}} = 3m_{\text{P}}^2; \quad (3.12)$$

3.3.2. The freeze-out procedure. In the case of the equilibrium production, an accurate solution of eq. (3.11) can be achieved, introducing the notion of freeze-out temperature, $T_F = T(x_F) = x_F m$ [9, 54]. Let us assume, initially, that $x_I < x_B$. We study eq. (3.11) in the two extreme regimes:

At very early times, when x_F, Y 's are very close to equilibrium. So, it is more convenient to rewrite eq. (3.11) in terms of the variable $(x) = Y(x) \frac{Y^{\text{eq}}(x)}$ as follows:

$$\frac{d}{dx} \left(Y^{\text{eq}0} + y_{\text{hvi}}(x) + 2Y^{\text{eq}} \right) = \frac{P}{g_q} \quad (3.13)$$

The freeze-out point x_F can be defined by

$$\left(\frac{d}{dx} \right)_{x_F} = \frac{Y_F Y^{\text{eq}}(x_F)}{Y^{\text{eq}}(x_F)} \left(\frac{d}{dx} \right)_{x_F} + 2Y^{\text{eq}}(x_F) = \frac{P}{g_q} (Y_F + 2) Y^{\text{eq}2}(x_F); \quad (3.14)$$

where Y_F is a constant of order one, determined by comparing the exact numerical solution of eq. (3.11) with the approximate under consideration one. Inserting eqs. (3.14) into eq. (3.13), we obtain the following equation, which can be solved w.r.t x_F iteratively:

$$\ln Y^{\text{eq}}(x_F) = \frac{P}{g_q} \int_{x_F}^1 \frac{y_{\text{hvi}}(x) + 2Y^{\text{eq}}(x)}{Y^{\text{eq}}(x)} dx \quad (3.15)$$

$$Y_F = Y(x_F) \text{ and } \ln Y^{\text{eq}}(x_F) = x^0 \frac{1}{x^2} \left(\frac{3}{2x} \frac{g_s^0}{g_s} + \frac{15}{8P_2(1-x)} \right) \quad (3.16)$$

At late times, when $x_F, Y \ll Y^{\text{eq}}$ and so, $Y^2 \ll Y^{\text{eq}2}, Y^2$. Inserting this into eq. (3.11) and integrating the resulting equation from x_F down to 0, we arrive at:

$$(a) Y_0 = \frac{Y_F}{Z_F} + J_F \int_{x_F}^1 \frac{y_{\text{hvi}}}{P g_q} dx \quad (3.17)$$

$$Y_F = (Y_F + 1) Y^{\text{eq}}(x_F) \text{ with } Y^{\text{eq}}(x) = \frac{g}{g_s} \frac{45}{4} \frac{1}{2} x^{3=2} e^{1-x} P_2(1-x); \quad (3.18)$$

where the x dependence can be derived from eq.2(7b). Although not crucial, a choice $Y_F = 1.2 \pm 0.2$ assist us to approach better the precise numerical solution of eq. (3.11).

Let us now suppose that $x_B < x_I$. We have to specify if the freeze-out of χ occurs during the KD or RD epoch. To this end, we solve trialily eq. (3.16) with $g_q = 1$ and if the derived x_F is $x_F < x_I$, we conclude that indeed the decoupling occurs at the RD era. Y_0 is given by:

$$Y_0 = \frac{Y_{\text{RD}}}{Z_{\text{RD}}} + J_{F2} \int_{x_F}^1 \frac{y_{\text{hvi}}}{P g_q} dx \text{ with } Y_{\text{RD}} = \frac{Y_F}{Z_F} + J_{F1} \int_{x_F}^1 \frac{y_{\text{hvi}}}{P g_q} dx \quad (3.19)$$

$$(a) J_{F1} = \int_{x_F}^1 \frac{y_{\text{hvi}}}{P g_q} dx; \quad (b) J_{F2} = \int_{x_F}^1 \frac{y_{\text{hvi}}}{P g_q} dx \quad (3.20)$$

and Y_F is given by eq. (3.18). If the derived x_F is $x_F > x_I$, our initial guess is not self-consistent. We re-solve eq. (3.16) with g_q , given by eq. (3.8b). If the re-derived x_F is $x_F > x_I$, the decoupling occurs at the KD era and the formulae above, eqs. (3.17)-(3.18), is valid without modifications. If, nally, the re-derived x_F is $x_F < x_I$, the decoupling does not occur either during the KD era. In this case, we are obliged to impose $x_F = x_I$ in eq. (3.17b) and $Y_F = 0$ in eq. (3.18) in order to extract Y_0 via eq. (3.17a).

3.3.3. The CDM abundance. Our nal aim is the calculation of the current relic density, which is based on the well known formula [54]:

$$\Omega_{\chi}^0 = \frac{\rho_{\chi}^0}{\rho_c^0} = m_{\chi} s_0 Y_0 = \frac{\rho_{\chi}^0}{\rho_c^0} \quad h_0^2 = 2.741 \times 10^8 Y_0 m_{\chi} = \text{GeV} \quad (3.21)$$

The presence of $g_q > 1$ in eq. (3.15) and, mainly, (3.17b) or (3.20b) reduces J_F or J_{F2} , thereby increasing the value h_0^2 w.r.t the one obtained in the SC (i.e. with $g_q = 1$), $h_0^2|_{\text{SC}}$. The resulting enhancement can be estimated, by defining the quantity [40]:

$$\eta = \frac{h_0^2}{h_0^2|_{\text{SC}}} = \frac{h_0^2}{h_0^2|_{\text{SC}}} \quad (3.22)$$

4. APPLICATIONS

Our numerical investigation depends on the parameters:

$$; \quad ; H_I; m \quad ; h \nu_i:$$

For ease of reference we call the three first parameters q parameters, whereas the two later, CDM parameters. Recall that we use $q(\tau) = 0$ throughout and V_0 is adjusted so that eq. (2.33) is satisfied. Nonetheless, for definiteness and clarity, we give the used value of V_0 in the explicit examples of *gs.* 1, 2 and 4. In general, V_0 ranges between about 1 and 10^{19} , increases with τ and turns out to be $(\tau; H_I)$ -independent, for fixed τ and $q(\tau)$ or $q(N_S)$.

As regards the CDM parameters, we have to clarify that $h \nu_i$ can be derived from m and the residual (s)-particle spectrum, once a specific theory has been adopted. However, to keep our presentation as general as possible, we decide to treat m and $h \nu_i$ as unrelated input parameters (following our strategy in ref. [35]). Specifically, keeping in mind that the most promising CDM particle is the LSP, we focus our attention on the range:

$$200 \text{ GeV} \leq m \leq 500 \text{ GeV} : \quad (4.1)$$

The lower bound in eq. (4.1) arises roughly from the experimental constraints on the SUSY spectra (see, e.g., *g.* 23 of ref. [3]), whereas the upper is imposed in order the analyzed range to be possibly detectable in the future experiments (see, e.g. ref. [53]). On the other hand, we isolate two extreme cases which we encounter when we use the non-relativistic expansion in order to calculate $h \nu_i$:

$$(a) \quad h \nu_i = a \quad \text{or} \quad (b) \quad h \nu_i = bx : \quad (4.2)$$

The x dependence in eq. (4.2b) emerges in the case of a bino LSP [62] without coannihilations (CANs), whereas eq. (4.2a) gives more or less reliable results to all the others cases [6]–[8], [55]–[60]. The values of a and b can be restricted by applying the bounds of eq. (1.2). Comments on the naturalness of the required values are given in sec. 4.5.

The presentation of our results begins with the description of the evolution of the various quintessential quantities in sec. 4.1 and the allowed ranges of the corresponding parameters in sec. 4.2. In sec. 4.3, we illustrate the two kinds of the h_0^2 increase, due to the presence of the KD epoch and in sec. 4.4, we compare the results of our numerical and semi-analytical h_0^2 calculations. Finally, in sec. 4.5 we present areas compatible with eqs. (1.2).

4.1. EVOLUTION OF THE QUINTESSENTIAL QUANTITIES

We illustrate the cosmological history of the various quintessential quantities presenting some diagrams where in the x -axis, the parameter $\tau = \ln(1+z)$ varies from τ_I down to the late times, e.g. 10 [23, 25, 31]. Namely:

In *g.* 1-(a), we display q and q^0 versus τ for $\tau_I = 41, H_{\tau_I} = 10^{40}$ and $\beta = 0.5$ ($V_0 = 1:6 \cdot 10^6$). Solid lines [crosses] are obtained by numerically solving eq. (2.10) [applying the analytical expressions of sec. 2.2]. Despite their simplicity, our semi-analytical expressions in eqs. (2.20), (2.24) and (2.28), reproduce impressively the numerical evolution of q and q^0 .

In *g.* 1-(b), we draw \log_i versus τ for $\tau_I = 41, H_{\tau_I} = 10^{40}$ and two "extreme" (see *gs.* 3-(a) and (b)) values of β , $\beta = 0.1$ ($V_0 = 33.5$) (solid lines) or $\beta = 1.15$ ($V_0 = 1.35 \cdot 10^9$) (dashed lines). For $i = q$ (bold black lines), we show \log_q , computed by inserting in eq. (2.11b) the numerical solution of eqs. (2.10a) and (2.10b). For $i = A$ (thin black lines), we show \log_A derived from eq. (2.30). For $i = R + M$ (light grey line), we show \log_{R+M} , which is the logarithm of the sum of the contributions given by eqs. (2.8a) and (2.8b).

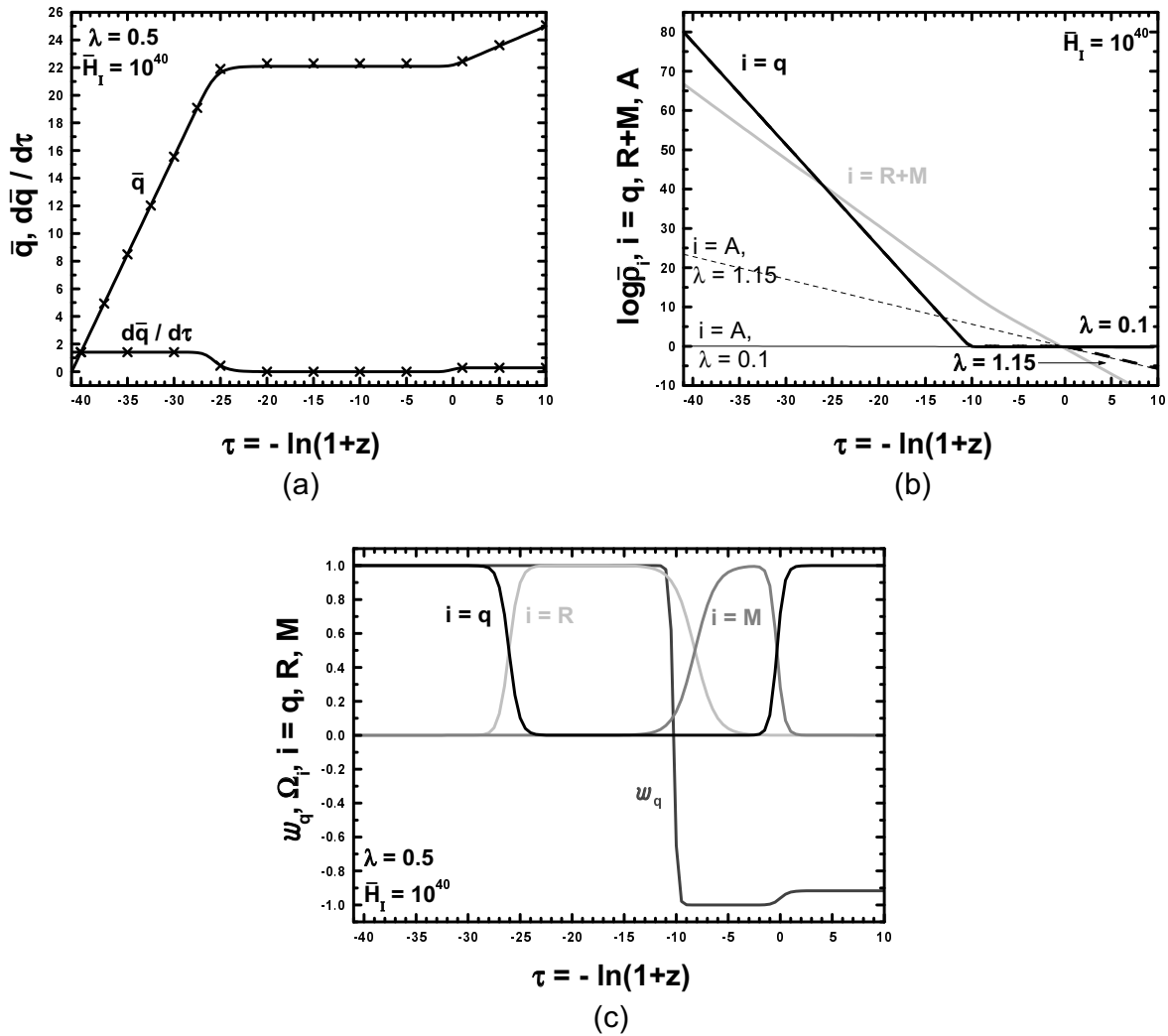


Figure 1: The evolution as a function of τ for $H_I = 10^{40}$ of the quantities: \bar{q} and $d\bar{q}/d\tau$ for $\lambda = 0.5$ ($V_0 = 1.6 \cdot 10^8$) (crosses are obtained by our analytical expressions) (a), $\log_{10} \bar{n}_i$ with $i = q$ (bold black lines), A (thin black lines) and $R+M$ (light grey line) for $\lambda = 0.1$ ($V_0 = 33.5$) (solid lines) or $\lambda = 1.15$ ($V_0 = 1.35 \cdot 10^{19}$) (dashed lines) (b), w_q (dark gray line) and Ω_i with $i = q$ (black line), R (light gray line) and M (gray line) for the values of $\lambda = 0.5$ ($V_0 = 1.6 \cdot 10^8$) (c).

In Fig. 1-(c), we plot w_q (dark gray line) and Ω_i with $i = q$ (black line), R (light gray line) and M (gray line) versus τ , for $H_I = 10^{40}$ and $\lambda = 0.5$ ($V_0 = 1.6 \cdot 10^8$). The y-axis quantities are computed by inserting in eqs. (2.14) and (2.13) the numerical values obtained by eqs. (2.11a), (2.11b) and (2.8).

Analyzing comparatively Figs. 2-(a), (b) and (c), we can demonstrate the characteristic features of the cosmological history in the presence of q . In particular:

- (i) For $\tau_{KR} = 26.2$, the universe undergoes the KD era. The field q increases according to eq. (2.20) along the left inclined part of the curve in Fig. 1-(a) and \bar{q} decreases, more steeply than \bar{n}_R , according to eq. (2.19), along the left inclined part of the black solid curve in Fig. 1-(b). During this period, $w_q = 1$, as shown in Fig. 1-(c). This era terminates at τ_{KR} , where an intersection of \bar{q} [Fig. 1-(a)] with \bar{n}_R [Fig. 1-(b)] is observed in Fig. 1-(b) [Fig. 1-(c)].

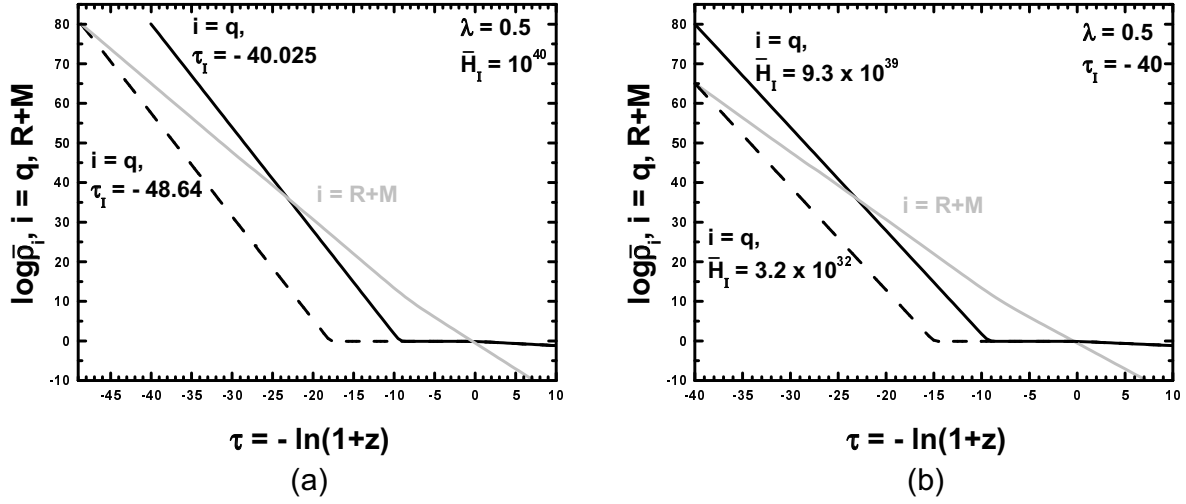


Figure 2: The evolution of the quantities \log_i with $i = q$ (black lines) and $R+M$ (light grey line) as a function of τ for $\lambda = 0.5$ and: $H_I = 10^{40}$ and $\tau_I = -40.025$ ($V_o = 1.6 \cdot 10^9$) [$\tau_I = -48.64$ ($V_o = 2.3$)] (solid [dashed] line) (a), $H_I = 9.3 \cdot 10^{39}$ ($V_o = 1.6 \cdot 10^9$) [$\tau_I = -3.2 \cdot 10^{32}$ ($V_o = 2.3$)] (solid [dashed] line) (b).

- (ii) For $\kappa_R = 26.2$ $\tau_{FA} = 0.67$, the universe undergoes successively the RD era and then the MD era until the re-appearance of DE. More precisely, q freezes to its constant value $q_f = 22.4$ according to eq. (2.24) (or eq. (2.25) for $\kappa_F = 20.2$) along the horizontal part of the curve in g. 1-(a). $R > q$ increases towards 1 along the light gray line of g. 1-(c) and then decreases until $M = R$ at $eq = 8.16$, where a slight kink is observed in the light gray line of g. 1-(b). For $\kappa_F = 10.22$, $q < R$ continues to decrease steeply according to eq. (2.19), along the left inclined part of the black solid curve in g. 1-(b), while w_q continues to be 1 as shown in g. 1-(c). On the other hand, for $\tau_{PL} = \tau_{FA}$, q freezes to its constant value $q_f = V(q_f) = 0.62$ in g. 1-(b), while w_q transits from 1 to -1 as shown in g. 1-(c). At present, we obtain $w_q(0) = 0.96$, within the limits of from eq. (2.34).
- (iii) For $\tau_{FA} = 0.67$, the universe undergoes a q -dominated phase. The field q increases according to eq. (2.28) along the right inclined part of the curve in g. 1-(a), q decreases according to eq. (2.30) along the right inclined parts of the curves in g. 1-(b) for $\lambda = 0.1$ and 1.15, while w_q in g. 1-(c) tends to its fixed-point value for $\lambda = 0.5$, $w_q^{fp} = 0.92$. As shown in the same figure $w_q^{fp} = 1$, which identifies the late-time attractor.

Note that, contrary to the case with $\lambda > 2$ [40], the variation of λ does not affect essentially the position of the FD plateau but only changes the inclination of the AD curve.

The dependence of the q evolution on τ_I [H_I], can be easily concluded from g. 2-(a) [g. 2-(b)], where we plot for $\lambda = 0.5$, $\log q$ and \log_{R+M} versus τ . In g. 2-(a) [g. 2-(b)] we take $H_I = 10^{40}$ and $\tau_I = -40.025$ ($V_o = 1.6 \cdot 10^9$) (solid line) or $\tau_I = -48.64$ ($V_o = 2.3$) (dashed line) [$\tau_I = -40$ and $H_I = 9.3 \cdot 10^{39}$ ($V_o = 1.6 \cdot 10^9$) (solid line) or $H_I = 3.2 \cdot 10^{32}$ ($V_o = 2.3$) (dashed line)]. It is obvious that increasing τ_I or H_I , the left, black inclined line of the q -KD regime moves to the right and consequently, both $q(\tau_I)$ and $q(\tau_{NS})$ increase. So, an upper [lower] bound on τ_I or H_I can be extracted from eq. (2.32) [eq. (2.31)] (see, g. 3). The saturation of these equations is the origin of the chosen lower [upper] τ_I or H_I in g. 2.

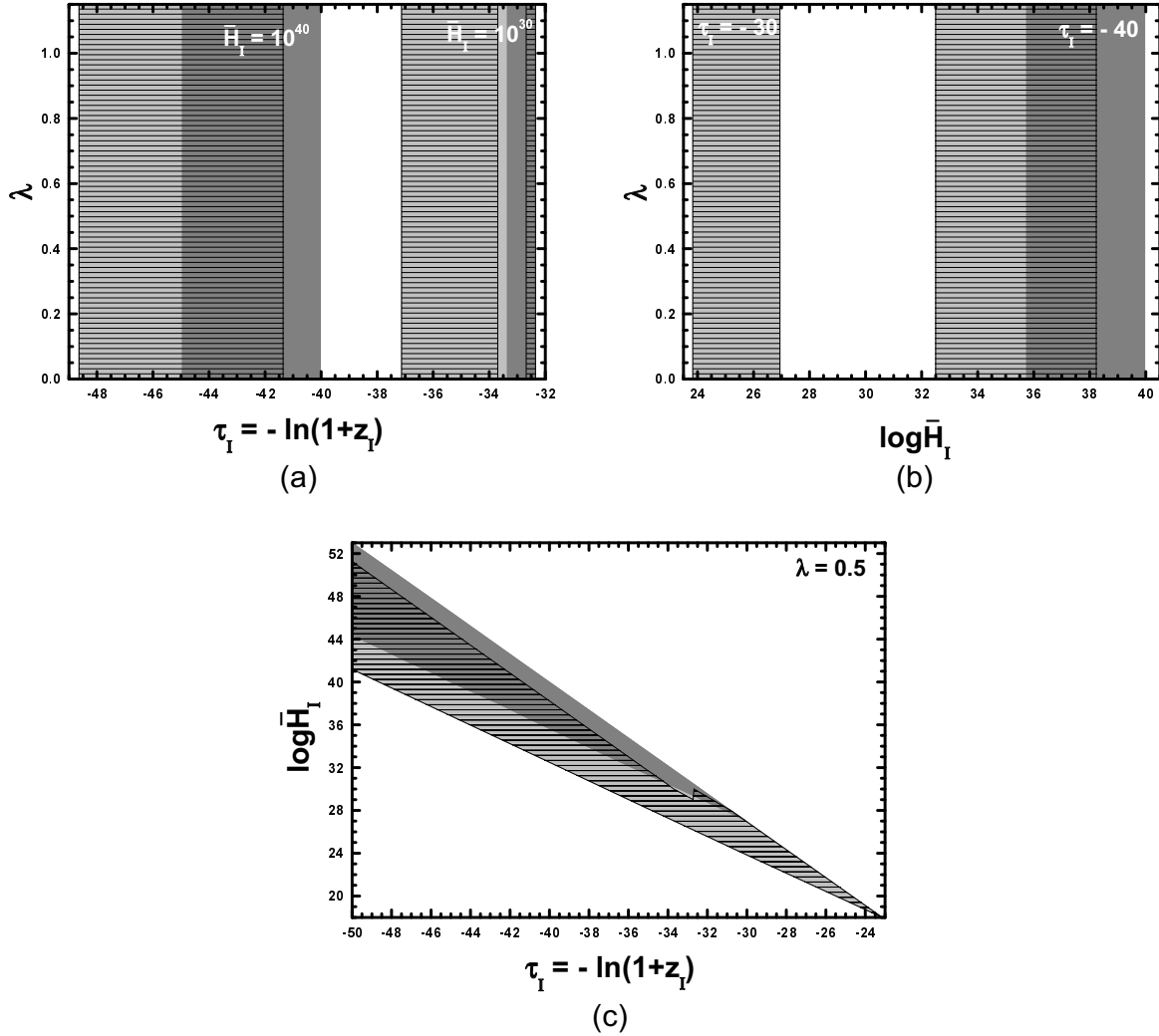


Figure 3: The allowed (shaded) areas on the τ_I plane for $H_I = 10^{40}$ or $H_I = 10^{30}$ (a), H_I plane for $\tau_I = 40$ or $\tau_I = 30$ (b) and $\log H_I$ plane for $\lambda = 0.5$ (c). Ruled area, also, the areas allowed by eq. (1.2b) for $m = 350$ GeV and $h_{\nu i} = 10^{-7}$ GeV $^{-2}$.

4.2. IMPOSING THE QUINTESSENTIAL REQUIREMENTS

We proceed, now in the delineation of the parameter space of our quintessential model. Agreement with eq. (2.34) entails $0 < \lambda < 1.15$ (see, also ref. [25]). This range is independent on τ_I and H_I as is shown in figs. 3-(a) and 3-(b). In these, we depict respectively the allowed (shaded) regions on the τ_I plane for $H_I = 10^{40}$ or $H_I = 10^{30}$ and on the $\log H_I$ plane for $\tau_I = 40$ or $\tau_I = 30$. In fig. 3-(c), we design the allowed area on the τ_I $\log H_I$ plane for $\lambda = 0.5$. The dark [light] shaded areas fulfill eq. (2.31b) [eq. (2.31a)]. The right [left] boundary curves of the allowed regions are derived from the saturation of eq. (2.32) [eq. (2.31a)] in figs. 3-(a) and 3-(b). The same origin has the upper [lower] boundary curve of the allowed region in fig. 3-(c), whereas the left boundary curve comes from eq. (2.35a). The construction of the ruled areas is explained in sec. 4.5.2. It is obvious that the decoupling, which occurs at $T_F = m = 20$ [9] corresponding (via eq. (2.7b)) to $F = (32.4 - 33.5)$ (for m in the range of eq. (4.1)) can take place either before ($F < \tau_I$) or after ($\tau_I < F$) the onset of the KD era.

4.3. PRE-VERSUS POST-FREEZE-OUT h_0^2 ENHANCEMENT

Figure:	4-(a ₁ ;a ₂)	4-(b ₁ ;b ₂)
Input Parameters		
= 0.5; m = 350 GeV		
I	41	32.6
H _I	10 ⁴⁰	10 ³⁰
V _o	1.6 · 10 ⁶	7.5 · 10 ⁴
h _{vi} (GeV ²)	2.92 · 10 ⁷	1.53 · 10 ⁸
Output Parameters		
q _(NS)	0.0007	0.056
K _R	25.7	23.6
B	36.03	
F	32.9	32.7
F _{↓C}	32.6	32.7
h ₀ ²	0.115	
	126.8	6.51

Table 1: Input and output parameters for the two examples illustrated in gs. 4-(a, b).

presence of the KD era causes an efficient h_0^2 enhancement, $h_0^2 \downarrow_C = 126.8$, which we call "pre-freeze-out" (note that $h_0^2 \downarrow_C = 0.0009$).

On the contrary, in the case of gs. 4-(b), we use [higher] lower values for I [H_I], so as $F < I$. Also, $q_{(NS)}$ turns out to be higher. The decoupling is realized in the RD era, as if we had adopted the SC, $F = F \downarrow_C$, but before the termination of the KD regime, $F < I < K_R$. The h_0^2 enhancement, $h_0^2 \downarrow_C = 6.51$, which we call "post-freeze-out" (note that $h_0^2 \downarrow_C = 0.015$) is less efficient (thereby decreasing the requisite h_{vi}).

It is worth mentioning that if we had not taken into account that $F < I$ in the latter case, we would have obtained $h_0^2 \downarrow_C = 970$. Consequently, $h_0^2 \downarrow_C$ should not be considered as a single-valued function of $q_{(NS)}$ (or of the ratio $q = q_R$ at a point [30, 40]) for fixed m and h_{vi} . The hierarchy between F and I turns out to be crucial for a reliable result of h_0^2 (see, also, sec. 4.5.3). Although the $F < I$ hypothesis could be regarded as less natural within a more complete scenario [37, 38, 39], it can not be excluded [23, 25]. Note, finally, that the phenomenon of re-annihilation [36] is not observed in our cases.

4.4. NUMERICAL VERSUS SEMI-ANALYTICAL RESULTS

The validity of our semi-analytical approach can be tested by comparing its results for h_0^2 with those obtained by the numerical solution of eqs. (3.4). In addition, useful conclusions can be inferred for the behavior of h_0^2 as a function of our free parameters and the regions where each h_0^2 -enhancement mechanism can be activated. As is shown in gs. 2-(a) and 2-(b), the position of the inclined left part of the black line (corresponding to $\log q$) is affected crucially by a possible variation of I or H_I but not of m . Therefore, $q_{(NS)}$ and consequently, h_0^2 (see eqs. (3.10) and (3.8)) depend on I or H_I but not on m . So, we fix $m = 0.5$ and we investigate the influence of the I or H_I variation on h_0^2 .

The operation of the two fundamental phenomena described in our work (i.e. the decoupling during [before the commencement of] the KD era) are instructively displayed in gs. 4-(a) [gs. 4-(b)]. Namely, in gs. 4-(a₁;b₁), we depict $h_{vi} = s$ (dotted lines) and $h_{vi} = s \downarrow_C$ (for $g_q = 1$) (bold [thin] solid lines) versus h_{vi} . In gs. 4-(a₂;b₂), we plot $\log q$ [$\log R$] (black [light gray] line) versus h_{vi} . The needed for our calculation inputs and some key-outputs are comparatively listed in Table 1. In both cases, we take the same m (and so, B). For better comparison, we give, also, the point of the decoupling, in the case of the SC ($g_q = 1$), $F \downarrow_C$. By adjusting h_{vi} we achieve to extract the central h_0^2 in eq. (1.2).

In the case of gs. 4-(a), we use [lower] higher values for I [H_I], so as $I < F$. Also, $q_{(NS)}$ turns out to be lower. The decoupling is realized deeply within the KD regime, $I < F < K_R$ and $F < F \downarrow_C$. The

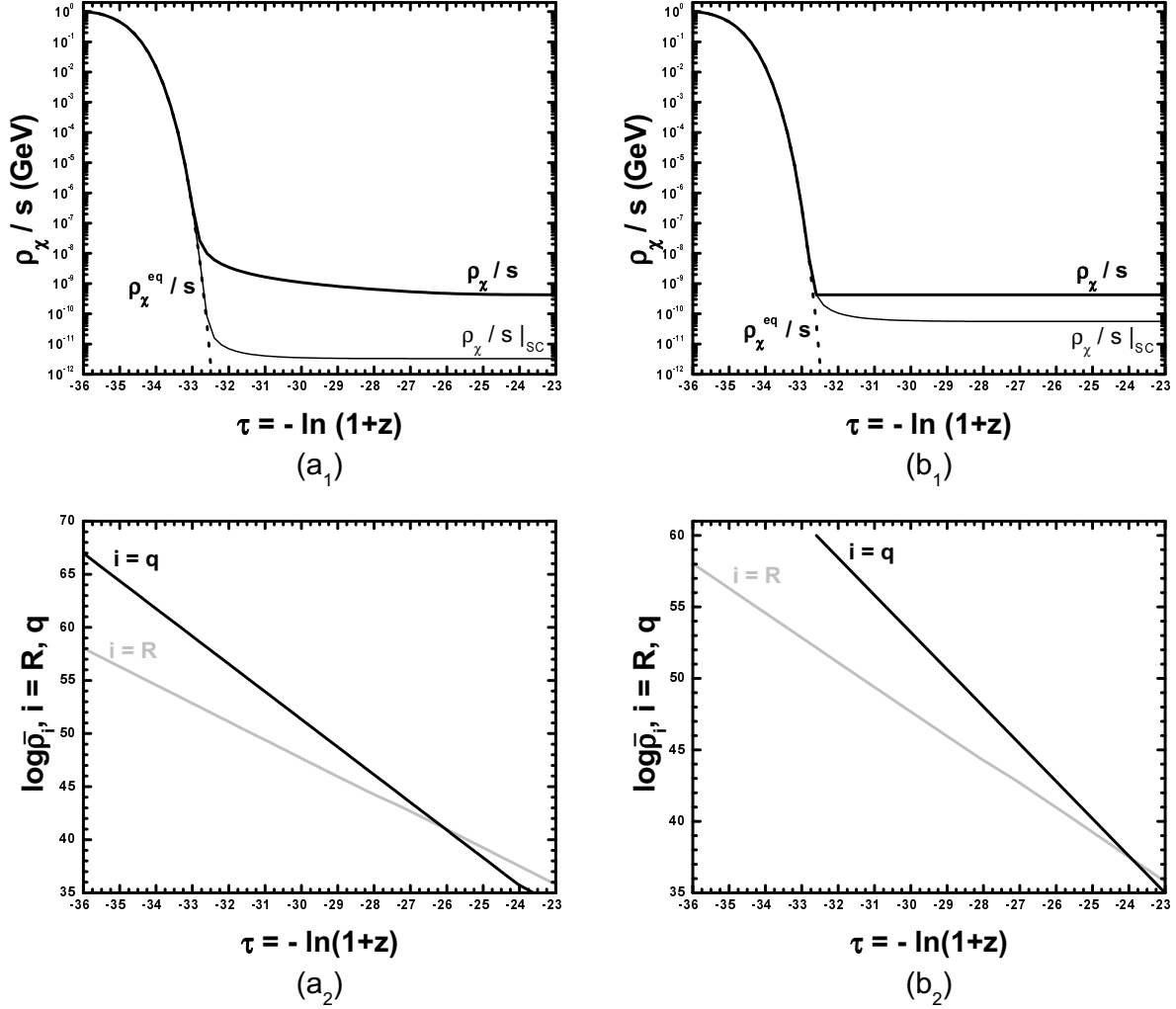


Figure 4: The evolution as a function of τ for $m = 350$ GeV and $\alpha = 0.5$ of the quantities ρ_χ^{eq}/s (dotted line) and ρ_χ/s (bold [thin] solid lines) for the quintessential scenario [SC] (a₁;b₁) and $\log_{10} \rho_i$ with $i = q$ [$i = R$] (black [light grey] line) (a₂;b₂). We take $\tau_I = 41$; $H_I = 10^{40}$ ($V_0 = 1.6 \cdot 10^8$) and $h_{\text{vi}} = 2.9 \cdot 10^{-7} \text{ GeV}^{-2}$ (a₁;a₂) for pre-freeze-out h_0^2 enhancement or $\tau_I = 32.6$; $H_I = 10^{30}$ ($V_0 = 7.5 \cdot 10^4$) and $h_{\text{vi}} = 1.53 \cdot 10^{-8} \text{ GeV}^{-2}$ (b₁;b₂) for post-freeze-out h_0^2 enhancement. In both cases, we extract $h_0^2 = 0.115$.

Our results are presented in figs. 5 and 6. The solid lines are drawn from our numerical code, whereas crosses are obtained by employing the method described in sec. 3.3 with $\tau_F = 128$ [$\tau_F = 135$] for $h_{\text{vi}} = 10^{10} \text{ GeV}^{-2}$ [$h_{\text{vi}} = 10^{10} \times \text{GeV}^{-2}$] in figs. 5-(a₁;a₂) [figs. 5-(b₁;b₂)] and 6-(a) [6-(b)]. The light [normal] grey lines and crosses correspond to $m = 200$ GeV [$m = 500$ GeV]. For these, we obtain $\tau_F' = 32.7$ [$\tau_F' = 33.7$], via eq. 3.15). In fig. 5, we design τ_I versus τ_I . In fig. 5-(a₁) and (b₁), we set $H_I = 10^{40}$. For any allowed τ_I (see fig. 3-(a)), we get $\tau_I < \tau_F$ and so, pre-freeze-out ρ_χ production. On the contrary, in figs. 5-(a₂) and (b₂), where we set $H_I = 10^{30}$, there is allowed (see fig. 3-(a)) $\tau_I > \tau_F$. At these points, we observe a sharp decrease of ρ_χ/s which signalizes the transition from the pre- to the post-freeze-out ρ_χ production. In figs. 6, we plot $\log_{10} \rho_i$ versus $\log H_I$, for $\tau_I = 40$ and $\tau_I = 30$. The allowed H_I 's (see fig. 3-(b)) are limited by vertical lines. For $\tau_I = 40$ [$\tau_I = 30$], we have $\tau_I < \tau_F$ [$\tau_F < \tau_I$] and so, pre[post]-freeze-out ρ_χ production.

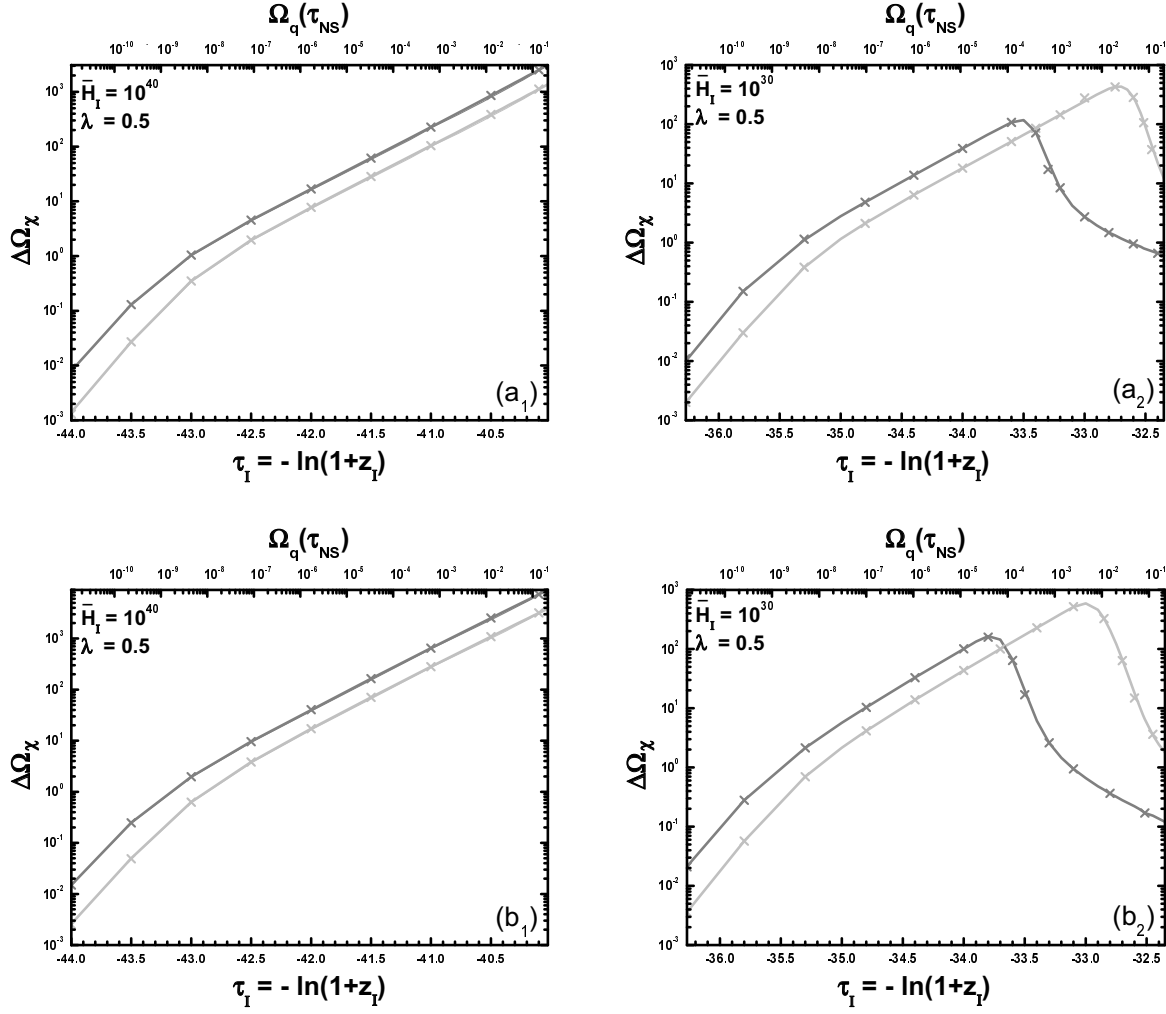


Figure 5: $\Delta\Omega_\chi$ versus τ_I or $g_q(\tau_{NS})$ for $H_I = 10^{40}$ (a₁; b₁) or $H_I = 10^{30}$ (a₂; b₂). We take $\lambda = 0.5$, $m = 200$ GeV [$m = 500$ GeV] (light [normal] grey lines and crosses) and $h \text{ vi} = 10^{-10}$ GeV² [$h \text{ vi} = 10^{-10} \times \text{GeV}^2$] (a₁; a₂ [b₁; b₂]). The solid lines [crosses] are obtained by our numerical code [semi-analytical expressions].

Comparing the results of figs. 5 and 6, we can deduce the behavior of $\Delta\Omega_\chi$ as a function of the parameters g_q ; m ; $h \text{ vi}$ for $\tau_I < \tau_F$ or $\tau_F < \tau_I$. These results can be understood more easily by simplifying the formulas of sec. 3.3.1. In particular, τ_F and $\Delta\Omega_\chi$ can be roughly estimated as:

$$(a) \quad \tau_F \approx \frac{P \overline{m}}{2 h \text{ vi}} \quad \text{and} \quad (b) \quad \frac{J_F j_c}{J_F} \approx 1 \quad \frac{P \overline{g_q}}{(1 - e^{-(\tau_I - \tau_F)})^2}; \quad \text{for } \tau_I < \tau_F \quad (4.3)$$

where we kept only the most important terms in eqs. (3.15), (3.16) and (3.12). Also, we have taken into account eqs. (3.17b) and (3.20), from which we extracted J_F $h \text{ vi} e^{-\tau_F} = \frac{P \overline{g_q}}{J_F j_c} h \text{ vi} e^{-\tau_F}$ and $J_{F1} h \text{ vi} (e^{-\tau_F} - e^{-\tau_I}) > J_{F2}$ (for constant $h \text{ vi} = a$).

Armed with these formulas, we can explain that $\Delta\Omega_\chi$ increases as:

- (i) g_q increases [decreases] (with fixed m and $h \text{ vi}$), for $\tau_I < \tau_F$ [$\tau_F < \tau_I$]. This is obvious from eq. (4.3b) for $\tau_I < \tau_F$. For $\tau_F < \tau_I$, an augmentation of g_q can be achieved, increasing τ_I , which results to a diminution of $\Delta\Omega_\chi$, via eq. (4.3b) (note that the shift of τ_F , given by eq. (3.15), due to g_q variation does not alter drastically the results).

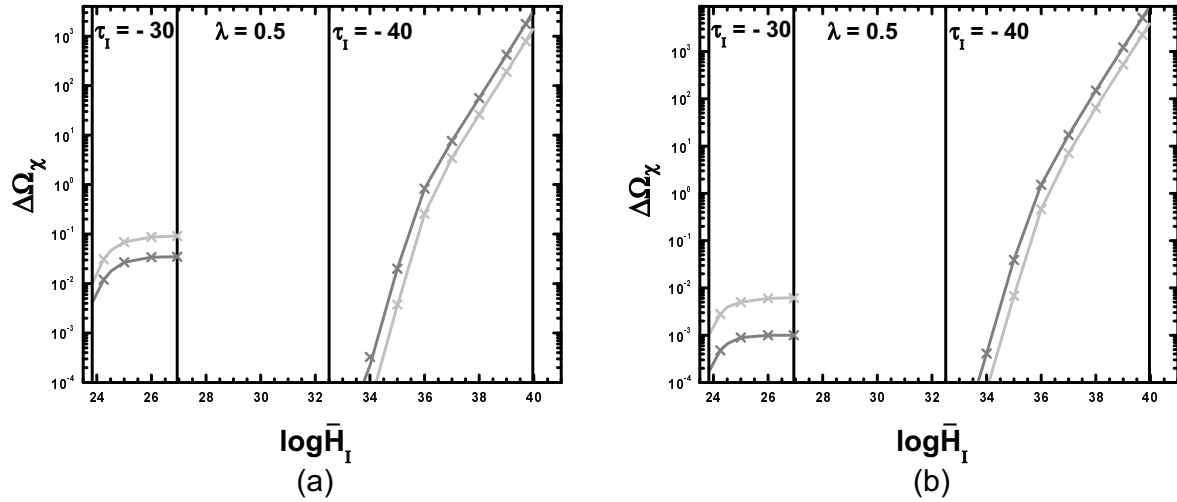


Figure 6: $\Delta\Omega_\chi$ versus $\log H_I$ for fixed (indicated in the graphs) τ_I . We take $\lambda = 0.5$, $m = 200 \text{ GeV}$ [$m = 500 \text{ GeV}$] (light [normal] grey lines and crosses) and $h\nu_i = 10^{-10} \text{ GeV}^{-2}$ [$h\nu_i = 10^{-10} \times \text{GeV}^{-2}$] (a [b]). The solid lines [crosses] are obtained by our numerical code [semi-analytical expressions]. The allowed regions on the $\log H_I$ axis are limited by vertical lines (compare with fig. 3-(b)).

- (ii) $h\nu_i$ decreases [increases] (with fixed m and g_q), for $\tau_I < \tau_F$ [$\tau_F < \tau_I$]. Indeed, from eq. (4.3a), decrease of $h\nu_i$ has as result a decrease of τ_F , which in turn, causes an increase [decrease] of τ_I for $\tau_I < \tau_F$ [$\tau_F < \tau_I$], as deduced from eq. (4.3b). Note that the case $h\nu_i = bx$ can be considered as a decrease of $h\nu_i = a$, since $x < x_F$ ($1=20$).
- (iii) m increases [decreases] (with fixed $h\nu_i$ and g_q), for $\tau_I < \tau_F$ [$\tau_F < \tau_I$]. Indeed, as shown from eq. (4.3a), an increase of m generates a decrease of τ_F which increases [decreases] τ_I for $\tau_I < \tau_F$ [$\tau_F < \tau_I$], as induced from eq. (4.3b).

Note, finally, that in all cases, the agreement between numerical and semi-analytical results is impressive, as is evident from figs. 5 and 6.

4.5. IMPOSING THE CDM REQUIREMENT

Requiring h_0^2 to be confined in the cosmologically allowed range of eq. (1.2), one can restrict the free parameters (the data is derived exclusively by the numerical program). This can be achieved systematically as follows:

4.5.1. Constraining the CDM parameters. Fixing the q parameters, we can derive restrictions on the CDM parameters. Namely, in fig. 7 we construct for $\lambda = 0.5$ the allowed regions on the m - $h\nu_i$ plane for $h\nu_i = a$ ($a; a_1; a_2$) or on the m - $h\nu_i = x$ plane for $h\nu_i = bx$ ($b; b_1; b_2$). The upper [lower] bounds of the allowed areas are derived from the saturation of eq. (1.2a) [eq. (1.2b)]. This is due to the fact that in any case, h_0^2 is inverse proportional to $h\nu_i$ as is obvious from eqs. (3.21) and (3.17) or (3.19) and so, h_0^2 decreases as $h\nu_i$ increases (contrary to the case of the non-equilibrium production [34, 35]).

In figs. 7-(a₁; b₁), we take $\tau_I = 41$ and $H_I = 10^{40}$ ($q_{(NS)} = 0.0007$). In this case, for any m in the range of eq. (4.1), $\tau_I < \tau_B$ and so, the pre-freeze-out mechanism of production is applied. We observe that, due to the presence of $g_q > 1$, τ_I increases with m more dramatically than in the case of the SC ($g_q = 1$), illustrated for reference in figs. 7-(a, b).

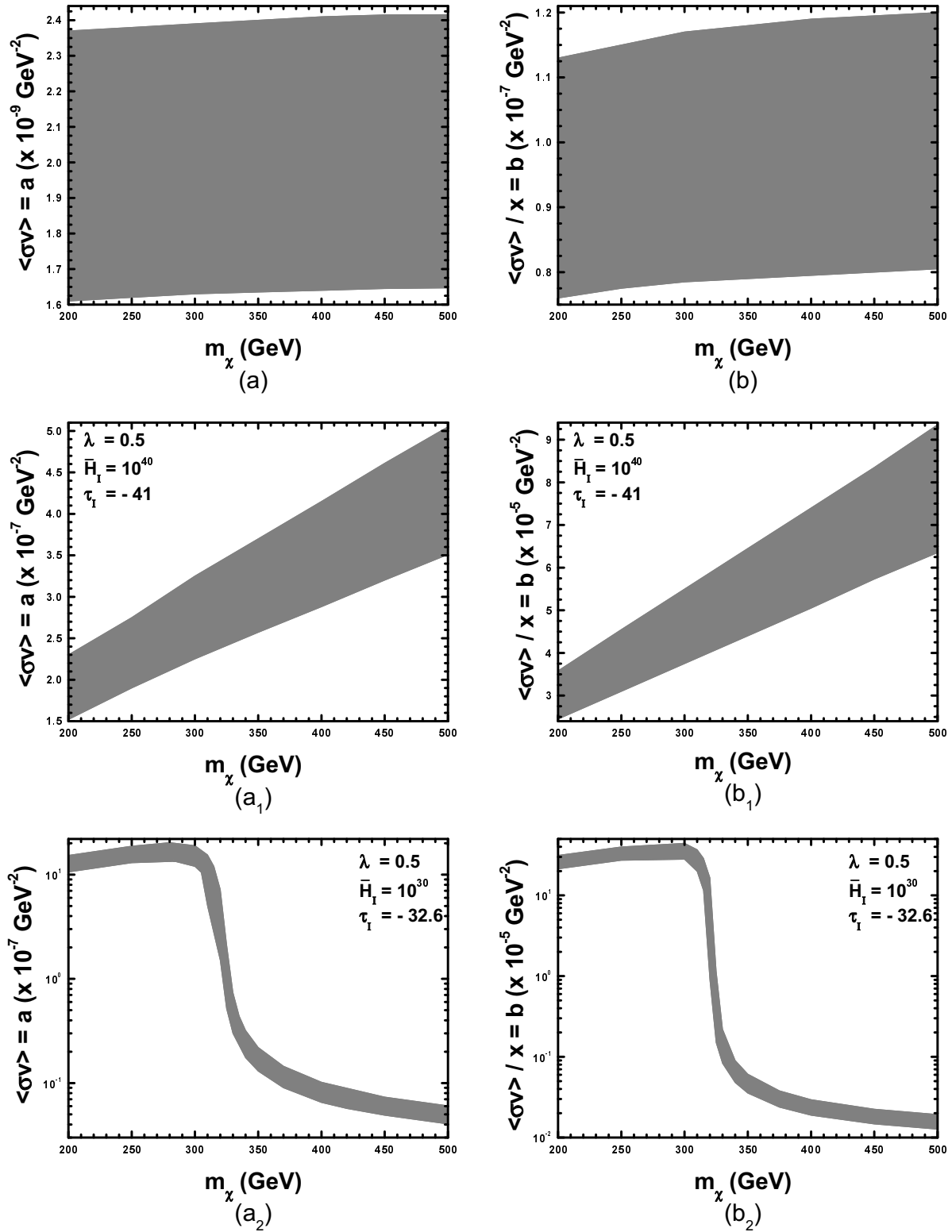


Figure 7: The allowed region on the m_χ - $h\nu_i$ plane for $h\nu_i = a$ (a; a₁; a₂) or on the m_χ - $h\nu_i/x$ plane for $h\nu_i = bx$ (b; b₁; b₂). We take $\lambda = 0.5$ and: $\tau_I = -41$ and $\bar{H}_I = 10^{40}$ (a₁; b₁) or $\tau_I = -32.6$ and $\bar{H}_I = 10^{30}$ (a₂; b₂), whereas, for the sake of comparison, we consider the SC ($g_{\text{SI}} = 1$) in gs. (a) and (b).

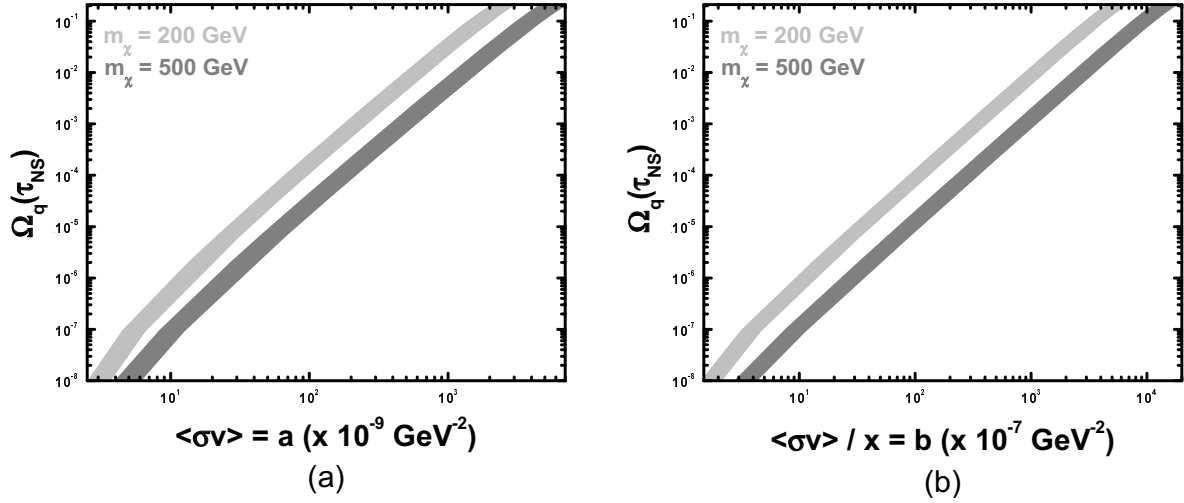


Figure 8: The allowed regions for $\Omega_q < \Omega_B$ and $m_\chi = 200 \text{ GeV}$ [$m_\chi = 500 \text{ GeV}$] (light [normal] grey areas) on the $h \nu_i - \Omega_q(\tau_{NS})$ plane for $h \nu_i = a$ (a) or on the $h \nu_i = x - \Omega_q(\tau_{NS})$ plane for $h \nu_i = bx$ (b).

In $gs. 7-(a_2; b_2)$, we take $\Omega_I = 32:6$ and $H_I = 10^{30}$ ($\Omega_q(\tau_{NS}) = 0:056$). At $m_\chi = 330 \text{ GeV}$ we obtain $\Omega_F = 32:6 = \Omega_I$ (via eq. (3.15)) and so, we observe a "transition" from the pre- to the post-freeze-out h_0^2 enhancement. As a result, for $m_\chi = 330 \text{ GeV}$ [$m_\chi = 330 \text{ GeV}$], the pre-freeze-out [post-freeze-out] mechanism of χ production is activated and consequently, large values for $h \nu_i$ (larger than those in $gs. 7-(a_1; b_1)$, since $\Omega_q(\tau_{NS})$ is larger) [two orders of magnitude lower values for $h \nu_i$] are needed such that eq. (1.2) is attained.

The requisite high values for $h \nu_i$ in the case of the pre-freeze-out χ production can be obtained by resorting to SUSY models which ensure A-pole effects [60, 61] or "gaugino-inspired" CANs [56, 57, 58], as in the applications [42, 43] of ref. [40]. Less efficient augmentation of $h \nu_i$ (which, although not suitable for the pre-freeze-out χ production, may be adequate for the post-freeze-out one) can be achieved by lowering the masses of the CDM candidates in ED models [6, 7, 8] or by employing fermionic CANs [55, 59, 58] in SUSY models. Consequently, the constrained minimal SUSY model [62], although tightly restricted even in the SC [61, 63], can be consistent with a quintessential KD period, e.g. applying the A-pole effects [60, 61] or in the case of the post-freeze-out χ production.

4.5.2. Constraining further the q parameters. Fixing the CDM parameters to naturally obtainable values, $m_\chi = 350 \text{ GeV}$ and $h \nu_i = 10^7 \text{ GeV}^{-2}$ (with $h_0^2 \approx 0:0025$), we can constrain further the q parameters. We require, for simplicity, the fulfillment of eq. (1.2b), which, in turn, is more rigorous than the eq. (1.2a), since other production mechanisms of χ may be activated [35, 64] and/or other CDM candidates [4] may contribute to Ω_{CDM} .

The regions consistent with the achievement of eq. (1.2b) are ruled in $g. 3$. Specifically, in $g. 3-(a)$, for $H_I = 10^{40}$ [$H_I = 10^{30}$], we have $\Omega_I < \Omega_F$ [$\Omega_I < \Omega_F$ or $\Omega_I > \Omega_F$] (where $\Omega_F = 32:9$ for $m_\chi = 350 \text{ GeV}$) and so, we obtain pre-freeze-out [pre- or post-freeze-out] χ production. Since Ω_q decreases as Ω_I (or g_q) increases (see sec. 4.4), a disconnected to the one with low Ω_I 's area arises for high Ω_I 's. In $g. 3-(b)$, for $\Omega_I = 30$ [$\Omega_I = 40$], we have $\Omega_F < \Omega_I$ [$\Omega_I < \Omega_F$] and consequently, pre-freeze-out [post-freeze-out] χ production. In $g. 3-(c)$, we observe an angle for $\Omega_I = \Omega_F$, where allowed areas of the type in $g. 3-(b)$ for $H_I = 10^{30}$ appear.

Interestingly, $\Omega_q(\tau_{NS})$ turns out to be constant and equal to 9×10^5 along the right

boundary curves of the [rst] ruled areas in g. 3-(a) for $H_I = 10^{40}$ [$H_I = 10^{30}$], in g. 3-(b) for $\alpha = 40$ and in g.3-(c) along the inclined upper boundary curve of the ruled area until the commencement of the angle. This observation pushes us to the construction of the next subsection's plots.

4.5.3. Constraining further $g_q(n_s)$. In the $\alpha < \beta$ case, the number of the free q parameters which determine h_0^2 can be reduced by one, since only g_q is involved in the h_0^2 calculation (see eqs. (3.21) and (3.17)), contrary to the $\beta < \alpha$ case, in which the h_0^2 calculation explicitly depends on α , also (see eq. (3.21) and (3.19)). In particular, $(\alpha; H_I)$ can be replaced by $g_q(n_s)$ (see eq. (3.10)). Obviously, e.g. from g. 3-(c), we observe that there is an infinite set of $(\alpha; H_I)$'s, which produce identical $g_q(n_s)$'s. So, it would be interesting to delineate the allowed parametric space, for $\alpha < \beta$ on the h vs $g_q(n_s)$ plane.

This aim is realized in gs. 8-(a) and (b). The light [normal] grey regions are constructed for $m = 200$ GeV [$m = 500$ GeV]. Lower m 's require lower h vs's, since α diminishes with m as we explain in sec. 4.4. Also, the upper [lower] bounds of the allowed areas are derived from the saturation of eq. (1.2a) [eq. (1.2b)], for the reason already mentioned in sec. 4.5.1. The importance of this graph is that given the CDM parameters and the fact that $\alpha < \beta$, restrictions supplementary to eq. (2.32) on $g_q(n_s)$ can be derived from eq. (1.2) non-dependent on the specific quintessential model.

5. CONCLUSIONS-OPEN ISSUES

We studied the cosmological evolution of a scalar field q which rolls down its exponential potential ensuring an early KD epoch and acting as quintessence today. We then investigated the decoupling of a CDM candidate, χ , during the KD epoch or before its commencement and calculated the χ -relic density. We solved the problem (i) numerically, integrating the differential equations which govern the cosmological evolution of q and the χ -number density (ii) semi-analytically, producing approximate relations for the former quantities. The second way facilitates the understanding of the problem and gives, in all cases, accurate results.

The parameters of the quintessential model are constrained by using the current observational data originating from nucleosynthesis, acceleration of the universe and the DE density parameter. We then analyzed the variation of the h_0^2 enhancement w.r.t the quintessential parameters in both regimes of χ decoupling demonstrating that the pre-freeze-out h_0^2 enhancement turns out to be much more efficient than the post-freeze-out one. Taking representative values for quintessential parameters, we constructed regions consistent with the present CDM bounds constraining h vs to rather high values, especially in the case of the pre-freeze-out h_0^2 enhancement. Alternatively, in the latter case, we showed that model-independent restrictions on quintessential density parameter at the eve of nucleosynthesis can be derived by enforcing the CDM constrain.

Our formalism could become applicable to other more elaborated quintessential models [28, 31, 36]. Also, it could be easily extended, in order to include coannihilations and/or A -pole effects for the h_0^2 calculation in the context of specific SUSY or ED models. In the latter case, novel deviations [10] from the SC arise, which could be similarly analyzed (although the brane-tension is to be rather low in order numerically visible changes on the h_0^2 calculation to be observable [11]). Lastly, low reheating scenarios [34, 35, 64] could become extremely appealing in the presence of quintessence, since they succeed to reduce h_0^2 without need of tuning the particle-model parameters. On the other hand, their coexistence with the quintessential evolution deserves certainly deeper investigation [65].

ACKNOWLEDGMENTS

The author would like to thank K. Dimopoulos, U. Franca and G. Lazarides for enlightening communications, the Greek State Scholarship Foundation (I. K. Y.) and the European Network ENTAP under contract RIICT-2004-506222 for financial support.

REFERENCES

- [1] D.N. Spergel et al, *Astrophys. J. Suppl.* 148, 175 (2003) [astro-ph/0302209].
- [2] M. Tegmark et al, *Phys. Rev. D* 69, 103501 (2004) [astro-ph/0310723];
A.G. Riess et al, *Astrophys. J. Suppl.* 607, 665 (2004) [astro-ph/0402512].
- [3] For a review from the viewpoint of particle physics, see
A.B. Lahanas et al, *Int. J. Mod. Phys. D* 12, 1529 (2003) [hep-ph/0308251].
- [4] For a review, see E.A. Baltz, astro-ph/0412170.
- [5] H.G. Goldberg, *Phys. Rev. Lett.* 50, 1419 (1983);
J.R. Ellis et al, *Nucl. Phys. B* 238, 453 (1984).
- [6] G. Servant and T.M.P. Tait, *Nucl. Phys. B* 650, 391 (2003) [hep-ph/0206071];
H.C. Cheng et al, *Phys. Rev. Lett.* 89, 211301 (2002) [hep-ph/0207125].
- [7] K. Agashe and G. Servant, *Phys. Rev. Lett.* 93, 231805 (2004) [hep-ph/0403143].
- [8] J.A.R. Cembranos et al, *Phys. Rev. Lett.* 90, 241301 (2003) [hep-ph/0302041];
Phys. Rev. D 68, 103505 (2003) [hep-ph/0302062].
- [9] E.W. Kolb and M.S. Turner, *The Early Universe*, Redwood City, USA: Addison-Wesley (1990).
- [10] P. Binetruy, C. Deffayet and D. Langlois, *Nucl. Phys. B* 565, 269 (2000) [hep-th/9905012].
- [11] N. Okada and O. Seto, *Phys. Rev. D* 70, 083531 (2004) [hep-ph/0407092];
T. N. Ihei, N. Okada and O. Seto, hep-ph/0409219.
- [12] M.S. Turner, *Phys. Rev. D* 33, 889 (1986).
- [13] J. Ellis, K.A. Olive, Y. Santoso and V.C. Spanos, *Phys. Lett. B* 588, 7 (2004) [hep-ph/0312262].
- [14] L. Covi et al, *J. High Energy Phys.* 06, 003 (2004) [hep-ph/0402240].
- [15] X.J. Bi, M. Li and X. Zhang, *Phys. Rev. D* 69, 123521 (2004) [hep-ph/0308218].
- [16] R.R. Caldwell et al, *Phys. Rev. Lett.* 80, 1582 (1998) [astro-ph/9708069].
- [17] P. Binetruy, *Int. J. Theor. Phys.* 39, 1859 (2000) [hep-ph/0005037];
V. Sahni, astro-ph/0403324.
- [18] B. Spokoiny, *Phys. Lett. B* 315, 40 (1993) [gr-qc/9306008];
M. Joyce, *Phys. Rev. D* 55, 1875 (1997) [hep-ph/9606223].
- [19] D. Comelli, M. Pietroni and A. Riotto, *Phys. Lett. B* 571, 115 (2003) [astro-ph/0302080];
U. Franca and R. Rosenfeld, *Phys. Rev. D* 69, 063517 (2004) [astro-ph/0308149].
- [20] A.L. Boyle et al, *Phys. Lett. B* 545, 17 (2002) [astro-ph/0105318];
R. Mainini and S.A. Bonometto, *Phys. Rev. Lett.* 93, 121301 (2004) [astro-ph/0406114].
- [21] J.P. Uzan, *Phys. Rev. D* 59, 123510 (1999) [gr-qc/9903004];
F. Perrotta et al, *Phys. Rev. D* 61, 023507 (2000) [astro-ph/9906066];
N. Bartolo and M. Pietroni, *Phys. Rev. D* 61, 023518 (2000) [hep-ph/9908521].
- [22] S.M. Carroll, *Phys. Rev. Lett.* 81, 3067 (1998) [astro-ph/9806099];
S. Lee, K.A. Olive and M. Pospelov, *Phys. Rev. D* 70, 083503 (2004) [astro-ph/0406039].
- [23] U. Franca and R. Rosenfeld, *J. High Energy Phys.* 10, 015 (2002) [astro-ph/0206194].
- [24] J. Weller and A. Albrecht, *Phys. Rev. D* 65, 103512 (2002) [astro-ph/0106079].
- [25] C.L. Gardner, *Nucl. Phys. B* 707, 278 (2005) [astro-ph/0407604].
- [26] P. Binetruy, *Phys. Rev. D* 60, 063502 (1999) [hep-ph/9810553];
A. Masiero, M. Pietroni and F. Rosati, *Phys. Rev. D* 61, 023504 (2000) [hep-ph/9905346].
- [27] P.J. Steinhardt, L. Wang and I. Zlatev, *Phys. Rev. Lett.* 82, 896 (1999) [astro-ph/9807002];
Phys. Rev. D 59, 123504 (1999) [astro-ph/9812313].
- [28] P. Brax and J. Martin, *Phys. Lett. B* 468, 40 (1999) [astro-ph/9905040];
P. Brax, J. Martin and A. Riazuelo, *Phys. Rev. D* 64, 083505 (2001) [hep-ph/0104240].
- [29] E.J. Copeland, A.R. Liddle and D. Wanders, *Phys. Rev. D* 57, 4686 (1998) [gr-qc/9711068];
E.J. Copeland, N.J. Nunes and F. Rosati, *Phys. Rev. D* 62, 123503 (2000) [hep-ph/0005222].
- [30] P. Salati, *Phys. Lett. B* 571, 121 (2003) [astro-ph/0207396].

- [31] F. Rosati, *Phys. Lett. B* 570, 5 (2003) [hep-ph/0302159].
- [32] C. Wetterich, *Nucl. Phys. B* 302, 668 (1988).
- [33] J.M. Cline, *J. High Energy Phys.* 08, 035 (2001) [hep-ph/0105251];
C. Kolda and W. Lahneman, hep-ph/0105300.
- [34] G.F. Giudice, E.W. Kolb and A. Riotto, *Phys. Rev. D* 64, 023508 (2001) [hep-ph/0005123];
N. Fornengo, A. Riotto and S. Scopel, *Phys. Rev. D* 67, 023514 (2003) [hep-ph/0208072].
- [35] C. Pallis, *Astropart. Phys.* 21, 689 (2004) [hep-ph/0402033].
- [36] R. Catena et al, *Phys. Rev. D* 70, 063519 (2004) [astro-ph/0403614].
- [37] P. J. Peebles and A. Vilenkin, *Phys. Rev. D* 59, 063505 (1999) [astro-ph/9810509];
M. Peloso and F. Rosati, *J. High Energy Phys.* 12, 026 (1999) [hep-ph/9908271].
- [38] M. Yahiro et al, *Phys. Rev. D* 65, 063502 (2002) [astro-ph/0106349].
- [39] K. Dimopoulos and J.W. Valle, *Astropart. Phys.* 18, 287 (2002) [astro-ph/0111417];
K. Dimopoulos *Phys. Rev. D* 68, 123506 (2003) [astro-ph/0212264].
- [40] S. Profumo and P. Ullio, *J. Cosm. & Astropart. Phys.* 11, 006 (2003) [hep-ph/0309220].
- [41] P.G. Ferreira and M. Joyce, *Phys. Rev. D* 58, 023503 (1998) [astro-ph/9711102].
- [42] U. Chattopadhyay and D.P. Roy, *Phys. Rev. D* 68, 033010 (2003) [hep-ph/0304108].
- [43] T. Ghregghetta, G.F. Giudice and J.D. Wells, *Nucl. Phys. B* 559, 27 (1999) [hep-ph/9904378].
- [44] G. Belanger et al, *Comput. Phys. Commun.* 149, 103 (2002) [hep-ph/0112278];
G. Belanger, F. Boudjema, A. Pukhov and A. Semenov, hep-ph/0405253.
- [45] P. Gondolo et al, *J. Cosm. & Astropart. Phys.* 07, 008 (2004) [astro-ph/0406204].
- [46] M. Hindmarsh and O. Philipsen, hep-ph/0501232.
- [47] R.H. Cyburt, B.D. Fields, K.A. Olive and E. Skillman, astro-ph/0408033.
- [48] R. Bean, S.H. Hansen and A. Melchiorri, *Phys. Rev. D* 64, 103508 (2001) [astro-ph/0104162];
Nucl. Phys. 110, (Proc. Suppl.) 167 (2002) [astro-ph/0201127].
- [49] M. Giovannini, *Phys. Rev. D* 60, 123511 (1999) [astro-ph/9903004];
V. Sahni, M. Sami and T. Souradeep, *Phys. Rev. D* 65, 023518 (2002) [gr-qc/0105121].
- [50] M.R. de Garcia Maia, *Phys. Rev. D* 48, 647 (1993);
M.R. de Garcia Maia and J.D. Barrow, *Phys. Rev. D* 50, 6262 (1994).
- [51] M. Yu. Khlopov and A.D. Linde, *Phys. Lett. B* 138, 265 (1984);
J. Ellis, J.E. Kim and D.V. Nanopoulos, *Phys. Lett. B* 145, 181 (1984).
- [52] C.L. Bennett et al, *Astropart. J.* 464, L1 (1996) [astro-ph/9601067].
- [53] For a review, see C. Muñoz, *Int. J. Mod. Phys. A* 19, 3093 (2004) [hep-ph/0309346].
- [54] P. Gondolo and G. Gelmini, *Nucl. Phys. B* 360, 145 (1991).
- [55] J. Ellis et al, *Astropart. Phys.* 13, 181 (2000) (E) *ibid.* 15, 413 (2001) [hep-ph/9905481];
M.E. Gomez, G. Lazarides and C. Pallis, *Phys. Rev. D* 61, 123512 (2000) [hep-ph/9907261].
- [56] J. Edsjo and P. Gondolo, *Phys. Rev. D* 56, 1879 (1997) [hep-ph/9704361].
- [57] A. Birkedal-Hansen and B.D. Nelson, *Phys. Rev. D* 67, 095006 (2003) [hep-ph/0211071].
- [58] C. Pallis, *Nucl. Phys. B* 678, 398 (2004) [hep-ph/0304047].
- [59] C. Boehm, A. Djouadi and M. Drees, *Phys. Rev. D* 62, 035012 (2000) [hep-ph/9911496];
J. Ellis, K. Olive and Y. Santoso, *Astropart. Phys.* 18, 395 (2003) [hep-ph/0112113].
- [60] A.B. Lahanas et al, *Phys. Rev. D* 62, 023515 (2000) [hep-ph/9909497];
J. Ellis et al, *Phys. Lett. B* 510, 236 (2001) [hep-ph/0102098].
- [61] M.E. Gomez, G. Lazarides and C. Pallis, *Nucl. Phys. B* 638, 165 (2002) [hep-ph/0203131];
C. Pallis and M.E. Gomez, hep-ph/0303098;
G. Lazarides and C. Pallis, hep-ph/0406081.
- [62] G.L. Kane et al, *Phys. Rev. D* 49, 6173 (1994) [hep-ph/9312272].
- [63] J. Ellis, K.A. Olive, Y. Santoso and V.C. Spanos, *Phys. Lett. B* 565, 176 (2003) [hep-ph/0303043];
H. Baer and C. Balazs, *J. Cosm. & Astropart. Phys.* 05, 006 (2003) [hep-ph/0303114];
A.B. Lahanas and D.V. Nanopoulos, *Phys. Lett. B* 568, 55 (2003) [hep-ph/0303130];
U. Chattopadhyay, A. Corsetti and P. Nath, *Phys. Rev. D* 68, 035005 (2003) [hep-ph/0303201].
- [64] T. Moroi and L. Randall, *Nucl. Phys. B* 570, 455 (2000) [hep-ph/9906527];
K. Kohri, M. Yamaguchi and J. Yokoyama, hep-ph/0502211.
- [65] A. Liddle and L.A. Urena-Lopez, *Phys. Rev. D* 68, 043517 (2003) [astro-ph/0302054].